Sādhanā (2020)45:52
https://doi.org/10.1007/s12046-020-1287-6

ANN-based optimization framework for performance enhancement of Restricted Access Window mechanism in dense IoT networks

MIRIYALA MAHESH* and V P HARIGOVINDAN

Department of Electronics and Communication Engineering, National Institute of Technology Puducherry, Karaikal, India
e-mail: miriyalamahesh4u@gmail.com; hari@nitpy.ac.in

MS received 8 February 2019; revised 11 September 2019; accepted 26 December 2019

Abstract. IEEE 802.11ah, marketed as Wi-Fi HaLow, operates at Sub 1 GHz spectrum to provide broad coverage, high throughput, energy efficiency and scalability. This makes IEEE 802.11ah a promising candidate for the Internet of Things (IoT). One of the major enhancements in the MAC layer is the Restricted Access Window (RAW) mechanism, which focuses on mitigating the channel contention in dense networks. The RAW mechanism reduces the channel contention among the group of devices by restricting their channel access to the allocated RAW slots. Since the standard does not specify the optimal RAW configuration parameters, choosing the number of RAW slots has significant impact on the performance of the RAW mechanism. In this paper, we develop an optimization framework by exploiting the Multilayer Perceptron Artificial Neural Network (MLP-ANN) to find the optimal number of RAW slots that can maximize the performance of the RAW mechanism in terms of throughput, delay and energy consumption. We train the ANN using the network size, Modulation and Coding Schemes, duration of the RAW period and the optimal number of RAW slots found using the analytical model presented in this paper. Further, we evaluate the performance of the RAW mechanism by choosing the optimal number of RAW slots provided by the ANN-based optimization framework. Results show that the proposed scheme significantly enhances the performance of the RAW mechanism. Finally, the analytical results are corroborated using extensive simulations done in ns-3.

Keywords. Internet of Things; IEEE 802.11ah; Restricted Access Window; Artificial Neural Network.

1. Introduction

The proliferation of communication devices unveils the evolution of the Internet of Things (IoT) to revolutionize the human–machine interaction. This paradigm has achieved a conceptual change in the wireless communications to enable the connectivity for exponentially increasing smart devices. IoT simplifies the interaction between the devices by enriching them with sensing, processing and networking capabilities. Thus, it supports several applications, including medical aids, intelligent transportation systems, disaster management, environmental monitoring, smart metering, wireless-controlled network and many others [1]. According to a forecast, 50 billion devices will be interconnected by 2020 [2]. To enhance the foreseen growth of IoT, a wireless network technology should provide high data rate, broad coverage, energy efficiency and extended scalability.

There exist many Low Power Wide Area Network (LPWAN) technologies like SigFox, DASH7, LoRaWAN, etc., to provide better coverage and throughput, but are limited in scalability. Alternatively, the 3GPP, LTE, WiMax, etc. can accommodate a large number of devices but consume more energy. To fill this gap, the Wi-Fi Alliance initiated the IEEE 802.11ah task group (TGah), with a motive to provide extended coverage, scalability and high throughput. This new standard operates in Sub-1-GHz (S1G) unlicensed ISM spectrum. Because of S1G, the standard can provide broad coverage of 1 km with data rates of at least 100 kbps and can associate up to 8192 devices [3].

Unlike the other IEEE 802.11 a/b/g/n/ac standards, IEEE 802.11ah inherits the physical layer of IEEE 802.11ac standard with the robust Modulation and Coding Schemes (MCS). It also introduces several enhancements to the MAC layer. The standard reduces the control overhead by implementing Null Data Packet (NDP) MAC frames, short MAC headers and management frames. To conserve energy consumption, Target Wake-Up Time and Traffic Indication Map segmentation are implemented. Scalability is improved using hierarchical Association Identifiers (AID) [4]. Above all, Restricted Access Window (RAW) mechanism is introduced to reduce the channel contention among the devices.

*For correspondence
Published online: 19 February 2020

The RAW mechanism groups the devices and allows each group of devices to contend for the channel in the restricted interval allocated to each group of devices. The restricted intervals or the RAW slots are periodically available to a group of devices. Choosing the number of RAW slots has significant impact on the performance of the RAW mechanism. Choosing the larger number of RAW slots, although decreases the contention among the devices, results in wastage of channel resources. Alternatively, less number of RAW slots increase the collisions and energy consumption. Hence, optimal number of RAW slots are required to enhance the performance of the RAW mechanism.

In this paper, we exploit the Multilayer Perceptron Artificial Neural Network (MLP-ANN) to determine the optimal number of RAW slots rather than solving the computationally complex non-linear analytical models [5–8]. ANN is a well-known nonlinear modelling method to solve complex industrial problems. It is widely used for pattern recognition, classification, function approximation, etc. The ANN is similar to the human brain in learning and decision-making process. It simulates the neural activity of the human brain to perform complex computations [9]. ANN has outstanding performance in generalizing the complex non-linear relationship between the input and output variables [10]. Among all the variants of ANN architectures, the feed-forward ANN with back propagation is the most robust architecture to approximate the output because of its simple structure, strong learning capability and high accuracy [11]. The ANN is trained with the network size, MCS, duration of the RAW period and the optimal number of RAW slots found using the analytical model presented in this paper. The trained ANN module is then used to find the optimal number of RAW slots for any set of input parameters.

The remainder of the paper is organized as follows. Section 2 presents the recent literature related to the performance of IEEE 802.11ah. Section 3 gives an overview of the major improvements of IEEE 802.11ah in PHY and MAC layer. The RAW mechanism is assessed using throughput, delay and energy consumption in section 4. An optimization framework is presented in section 5 to find the optimal number of RAW slots. Section 6 discusses the analytical and simulation results. Finally, we conclude our findings in section 7. The major contributions of the paper are summarized as follows:

- We present a simple yet accurate analytical model to evaluate the performance of the RAW mechanism in terms of throughput, delay and energy consumption.
- To reduce the computational overhead involved in solving the complex non-linear equation, we propose a novel optimization framework to find the optimal number of RAW slots (number of groups) using ANN. The ANN is trained using the network size, MCS, duration of the RAW period and the optimal number of RAW slots obtained using the analytical model.
- All the presented results show that the proposed optimization framework using ANN can provide the optimal number of RAW slots for various input conditions, which in turn significantly improves the throughput performance of the IEEE 802.11ah RAW mechanism.
- We compare the optimal number of RAW slots found in this article to the optimal number of RAW slots found using Simulated Annealing algorithm as well as the analytical approach by Park *et al* in [12].
- The analytical results are corroborated by extensive ns-3 simulations.

2. Literature survey

Ever since the IEEE 802.11ah is drafted, many works have been published to present the salient features, design challenges and enhancements in PHY and MAC layer of the protocol [13–15]. Authors of [15] assessed the performance of IEEE 802.11ah for various Machine to Machine (M2M) communication scenarios and explored the key features of the standard. Similarly, in [13] and [14], authors provided a detail description of significant enhancements introduced in the protocol.

In the literature, several works explored the various aspects of the physical layer in IEEE 802.11ah. Mostly, authors concentrate on the performance of the PHY layer and hardware implementation of the IEEE 802.11ah [16–18]. Hazmi *et al* in [16] studied the link budget, achievable data rates and packet size design for different channel conditions and suggested that IEEE 802.11ah can provide reliable communication link, better coverage and good throughput when compared with the existing solutions. Aust and Ito [17] studied the performance of different urban propagation path loss models under S1G frequency spectrum. Authors of [18] designed a programmable IEEE 802.11ah station based on the Cadence Xtensa digital signal processor.

Grouping mechanism is an active research area in IEEE 802.11ah. Although grouping the devices in the network reduces the contention in the network, it also results in the hidden terminal problem. To increase the network performance effectively, many works have been published [19–21]. In [19], the authors analysed the impact of the hidden node on the performance of the network and proposed the hidden node matrix-based grouping algorithm. According to their algorithm, the hidden nodes are alleviated by iterative regrouping of the nodes. Similarly, Damayanti *et al* [20] presented a grouping algorithm to obviate the hidden terminal problem by regrouping the nodes based on carrier sensitivity table. Dong *et al* [21] introduced an efficient grouping scheme based on the location of the device to reduce the influence of hidden terminals.

Many works focus on the performance of RAW mechanism and optimization of RAW parameters. The RAW parameters like duration of RAW period and the number of RAW slots have significant impact on the performance of the IEEE 802.11ah protocol. For example, choosing more number of RAW slots results in the wastage of channel resources and choosing less number of RAW slots increases the contention among the devices. Hence, many authors have focused on optimizing the RAW configuration parameters [12, 22–25]. Park *et al* [12] found the optimal size of RAW by establishing a relation between the average number of devices and the duration of the RAW slot. Similar to [12], authors in [23] and [24] proposed an energy-aware window control algorithm to optimize the energy efficiency based on the number of devices in the network and the number of RAW slots. Chang *et al* in [22] proposed a load balancing grouping scheme to improve the channel utilization in a heterogeneous network with different traffic constraints. In [25], the authors developed an analytical framework to evaluate the throughput by dividing the RAW duration into two sub-frames and selecting the duration of RAW slots according to the group size. Nurzaman *et al* [4] found the optimal duration of the RAW period based on the traffic loads and provided relay node support to use different MCS. Authors in [2] implemented a half-duplex decode and forward relay station between the access point and end device and analytically derived the achievable range for all the MCS. Correspondingly, Kocan *et al* [2] found the extended range using relay stations and suggested that a wide coverage can be achieved with the limitation of the throughput requirements of at least 100 kbps.

In [26], authors enhanced the throughput and energy efficiency using interference-aware dynamic frequency allocation scheme. Authors of [27] presented a novel sequential transmission scheme and provided an analytical model to evaluate the performance of S1G WLANs in the IoT environment. Tian *et al* [28] developed an IEEE 802.11ah module in ns-3 to find the optimal RAW grouping configuration under heterogeneous traffic conditions. Most of these optimization works are based on the probabilistic model and may introduce computational overhead at each node, which has limited processing capabilities. Hence, we propose a novel optimization framework using ANN to find the optimal number of RAW slots that can maximize the throughput, and minimize the delay and energy consumption of the IEEE 802.11ah network.

3. Overview of IEEE 802.11ah

With a motive to provide broad coverage, high throughput and energy efficiency, IEEE 802 LAN/MAN Standards Committee (LMSC) initiated IEEE 802.11ah task group under S1G spectrum of ISM frequency bands. To meet these requirements, the standard introduces significant enhancements in PHY and MAC layer, which are not present in the legacy IEEE 802.11 standards. In this section, we present the salient features of the protocol.

3.1 *PHY layer*

The IEEE 802.11ah inherits the basic physical layer of IEEE 802.11ac [29]. Besides operating under S1G spectrum, the physical layer of 802.11ac is 10 times down-clocked to provide five different channels of bandwidth 1, 2, 4, 8 and 16 MHz and followed by 10 different MCS. The available S1G spectrum differs for every country as shown in table 1. Besides the availability of different channels, the standard supports four spatial streams to provide various data rates with different ranges for diverse applications. For the 2 MHz channel, the PHY layer uses 64 tones/sub-carriers per OFDM symbol separated by 31.2 kHz. It also supports various modulations, including BPSK, QPSK and 16–256 QAM. In case of 1 MHz channel, 32 tones/sub-carriers are used per OFDM symbol [30].

Among all the five different channels, the 802.11ah radio should support 1 and 2 MHz, while the rest of them are optional. Table 2 shows all the MCS and corresponding data rates for the 2 MHz channel. In addition to this, the IEEE 802.11ah introduces MCS10 to provide wide coverage. The MCS10 scheme uses binary phase shift keying (BPSK) with 1/2 code rate at 1 MHz channel to provide longer range [31]. Following MCS10, MCS0 is the next most robust scheme to provide wide coverage. In an outdoor scenario, the transmission range exceeds 1 km if MCS10 is used, while it is 850 m using MCS0 for the transmission power of 200 mW [14].

3.2 *MAC layer*

Unlike the legacy IEEE 802.11 standards, IEEE 802.11ah introduces various enhancements in the MAC layer to increase the scalability and energy efficiency, and to decrease the contention in the network. In this section, we discuss a few developments in the MAC layer relevant to this research work.

3.2.1 *Scalability* IEEE 802.11ah expands the network size by assigning a unique AID to each device. It extends the connectivity up to 8192 devices by defining the hierarchical structure of AID. The structure of AID has 13 bits with a four-level hierarchy as shown in figure 1. The first 2 bits of AID represent a page index, the next 5 bits represent block index, etc.

3.2.2 *Power saving mechanism* Every device associated to an AP has a bit set in the virtual bitmap of

Table 1. IEEE 802.11ah spectrum availability in different countries.

Country	ISM frequency bands (MHz)	Power radiated (mW)	Channels (MHz)
China	614–787	5	1
	779–787	10	
Europe	863–868.6	10	1, 2
Japan	915.9–929.7	1, 20, 250	1
Singapore	866–869	500	1, 2, 4
	920–925		
South Korea	917–923.5	3, 10	1, 2, 4
United States	902–928	1000	1–16

Table 2. MCS and different data rates for 2 MHz channel.

MCS	Modulation	CR	Bits per OFDM symbol	Data rate (Mbps)
MCS0	BPSK	1/2	52	0.65
MCS1	QPSK	1/2	104	1.30
MCS2	QPSK	3/4	104	1.95
MCS3	16 QAM	1/2	208	2.60
MCS4	16 QAM	3/4	208	3.90
MCS5	64 QAM	2/3	312	5.20
MCS6	64 QAM	3/4	312	5.85
MCS7	64 QAM	5/6	312	6.50
MCS8	256 QAM	3/4	416	7.80

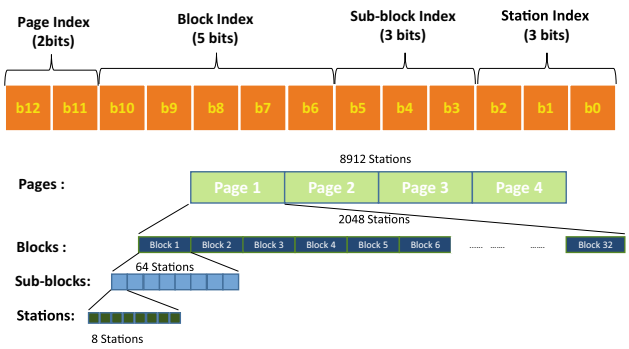

Figure 1. Hierarchical structure of AID.

TIM Information Elements to enable power saving mechanism. Broadcasting a TIM bitmap of length 8192 bits periodically drains the batteries of every device in the network. To overcome this problem, TGah defines TIM segmentation, i.e., the TIM bitmap is divided into several segments and broadcasted separately using TIM beacons. Generally, the beacon interval is the duration between two Delivery Traffic Indication Map (DTIM) beacons. Between the DTIMs, there will be multiple TIM beacons and between two consecutive TIM beacons, the channel time is divided into the RAW period and Contention Access Period (CAP). Each RAW period is again divided into multiple RAW slots as illustrated in figure 2. The DTIM beacon contains the bitmap of TIM segments so that each station wakes up during the corresponding TIM beacon. During each TIM beacon, the station that has a packet destined to it by the AP wakes up and contends for the channel access. Another feature to conserve the energy consumption is TWT. The devices that do not periodically transmit the data negotiate with the AP about their wake-up times, i.e., schedule their wake-up times, which may be from seconds to years.

3.2.3 *Channel access mechanism* Since the channel access time is divided into RAW period and CAP, each station maintains two back-off windows, one during the RAW period and the other during the CAP. During the CAP, all the devices contend for the channel using the DCF whereas Group Synchronized DCF (GS-DCF) is used for contention in the RAW period. The RAW mechanism is a group-based contention access mechanism to reduce the collision among the devices and to increase energy efficiency. It groups the devices and allows each group of devices to contend in a restricted interval or RAW slot using GS-DCF. GS-DCF is based on EDCA, i.e., the contention among the group of devices is restricted to a RAW slot where the rest of the devices enter into sleep

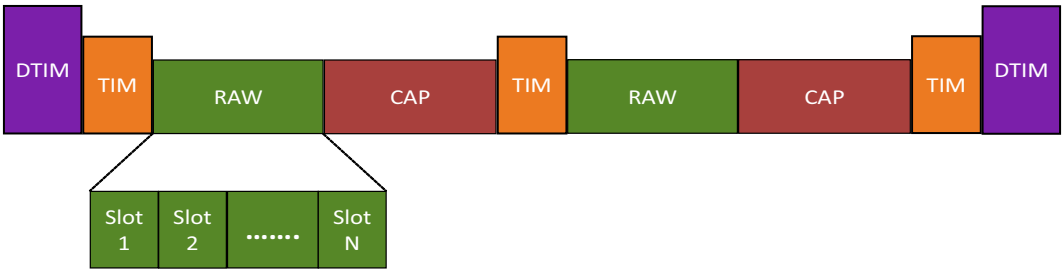

Figure 2. Duration of beacon interval.

mode. The AP is responsible for grouping. During the DTIM beacon, each device receives Raw Parameter Set Information Elements (RPS-IE), which contains the information about the AIDs of devices, duration of RAW slots and RAW start time. Using this information, each device finds the allocated RAW slot according to the following function:

$$\chi_{slot} = (AID_n + N_{offset}) \bmod L, \quad (1)$$

where χ_{slot} is the index of the slot allocated to the *nth* device, whose AID is AID_n, N_{offset} is the two least significant octets of the beacon frame (included for fairness) and L is the number of slots per RAW period.

There are two types of RAW mechanism: (i) generic RAW mechanism and (ii) triggered RAW mechanism. In the generic RAW mechanism, the AP assigns a RAW slot to every group of devices. However, in low-density networks, none of the devices may contend in a RAW slot, resulting in unused slots as shown in figure 3a, whereas in the high-density network, there will be at least one device ready to contend for the channel. This phenomenon reduces the performance of the RAW mechanism. To overcome this problem, triggered RAW mechanism is introduced. By enabling the resource allocation (RA) frame indication bit in the RAW type field, triggered RAW mechanism is activated. In this mechanism, the first RAW period is used to contend for slot reservation. The device that deserves a RAW slot is informed using RA frame. In the next RAW period, only the reserved RAW slot appears for contention. For example, as shown in figure 3b the devices that belong to group-1 and group-3 contend for slot reservation in the next RAW period by sending the PS_Poll request, while slot-2 and slot-4 are unused. After the first RAW period, the AP broadcasts RA frame, indicating the reservation of RAW slots for the respective devices. Hence only two RAW slots appear in the next RAW period. This mechanism reduces the wastage of channel resources, thus increasing the performance of the RAW mechanism.

Apart from this, the RAW mechanism defines two particular cases. The first is no crossing (NCR) slot, i.e., all the transmissions should end before the boundary of the RAW slot. This case provides a fair allocation of the channel, but also wastes the channel resources [13]. The second is crossing (CR) slot, i.e., the transmissions are allowed to cross the boundary of the RAW slot, which violates the fairness but effectively utilizes the channel resources.

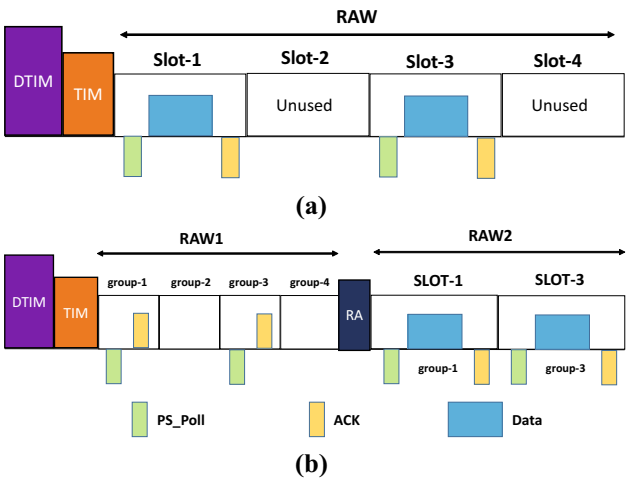

Figure 3. Types of RAW mechanism: (a) generic RAW mechanism and (b) triggered RAW mechanism.

4. Analytical model

This section presents an analytical model to assess the throughput, delay and energy consumption of IEEE 802.11ah RAW mechanism. We consider a network of size N divided into K groups such that each group has $g = \frac{N}{K}$ devices. For simplicity, we assume that all the devices in the network have saturated traffic and the channel is error-free. The duration of RAW period Δ_{RAW} is divided into several RAW slots of duration Δ_{slot} such that $\sum_{i=0}^{K} \Delta_{slot,i} = \Delta_{RAW}$. The channel is composed of mini-slots of duration ρ. We consider a scenario in which the AP employs uniform grouping scheme[1] with NCR case.

Each device in a group contends for the channel access using GS-DCF in a RAW slot. Every device in a RAW slot

[1]In uniform groping scheme the number of RAW slots is equal to the number of groups.

senses the channel for DIFS duration (δ_d) before contending for the channel and initializes a back-off counter from $(0, W_0 - 1)$, where W_0 is the minimum contention window (CW_{min}). The back-off counter doubles for every collision until it reaches a maximum contention window (CW_{max}). Otherwise, it resets to CW_{min} for either a successful packet transmission or the packet is dropped. Therefore, W_i is the contention window of the *ith* back-off stage and is given by

$$W_i = \begin{cases} 2^i W_0, & 0 \le i \le m-1, \\ 2^m W_0, & m \le i \le m', \end{cases} \tag{2}$$

where m is the maximum number of back-off stages and m' is the retransmission limit.[2]

A device gets a transmission opportunity[3] ($\xi = \Delta_{DATA} + \Delta_{ACK} + SIFS$) when the back-off counter decrements to zero. The duration of the RAW slot should be greater than the duration of a packet transmission ($\Delta_{slot} > \xi + \delta_d + \rho$) to ensure at least one transaction in a RAW slot.

Let $s(t)$ and $b(t)$ be the random process representing the back-off stage and back-off counter; let $\mathbb{P}_{t,j}$ and $\mathbb{P}_{c,j}$ be the packet transmission probability and collision probability in a mini-slot of a *jth* RAW slot, respectively. We model the bi-dimensional stochastic process $\{s(t), b(t)\}$ with discrete-time Markov chain as illustrated in figure 4.

Let $\mathfrak{U}_{i,k} = \lim_{t \longrightarrow \infty} \mathbb{P}\{s(t) = i, b(t) = k\},\ i \in [0, m],\ k \in [0, W_i - 1]$ be the stationary distribution of the Markov chain; then $\mathfrak{U}_{i,k}$ is calculated as

$$\mathfrak{U}_{i,0} = \mathbb{P}_{c,j} \mathfrak{U}_{i-1,0}, \quad 0 < i \le m, \tag{3}$$

$$\mathfrak{U}_{i,0} = \mathbb{P}^i_{c,j} \mathfrak{U}_{0,0}, \quad 0 < i \le m. \tag{4}$$

Due to chain regularities for each $k \in [1, W_i - 1]$, we have

$$\mathfrak{U}_{i,k} = \frac{W_i - k}{W_i} \mathfrak{U}_{i,0}, \quad i \in [0, m], \quad k \in [0, W_i - 1]. \tag{5}$$

Using Eqs. (3) and (5), we express all $\mathfrak{U}_{i,k}$ as a function of $\mathfrak{U}_{0,0}$, which depends on $\mathbb{P}_{c,j}$, m and m' [32]:

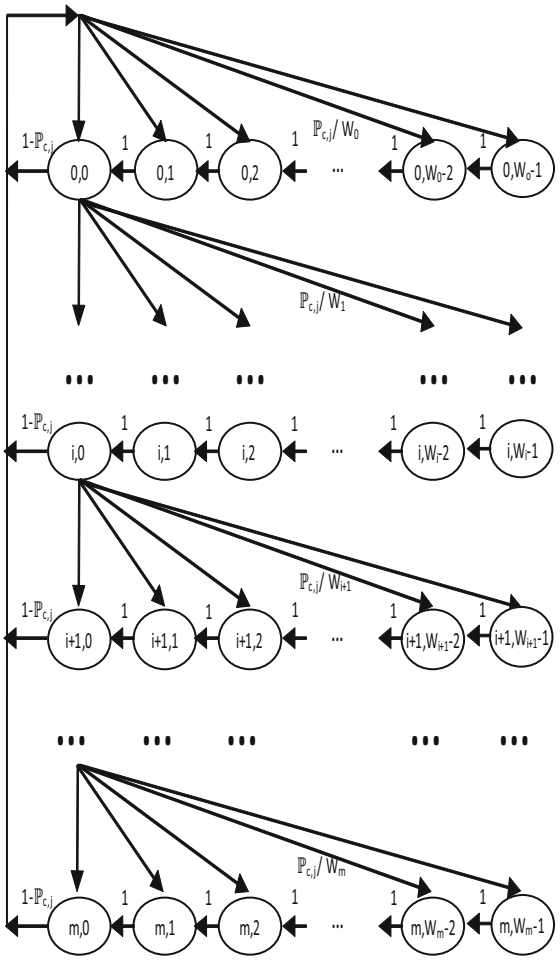

Figure 4. A bi-dimensional discrete-time Markov chain model.

$$\mathfrak{U}_{0,0} = \begin{cases} \dfrac{2(1-\mathbb{P}_{c,j})(1-2\mathbb{P}_{c,j})}{\left((1-2\mathbb{P}_{c,j})\left(1-\mathbb{P}_{c,j}^{m+1}\right) + W_0(1-(2\mathbb{P}_{c,j})^{m+1})(1-\mathbb{P}_{c,j})\right)}, & m \le m', \\ \dfrac{2(1-\mathbb{P}_{c,j})(1-2\mathbb{P}_{c,j})}{\left((1-2\mathbb{P}_{c,j})\left(1-\mathbb{P}_{c,j}^{m'+1}\right) + W_0(1-(2\mathbb{P}_{c,j})^{m'+1})(1-\mathbb{P}_{c,j}) + W_0 2^{m'}\mathbb{P}_{c,j}^{m'+1}(1-2\mathbb{P}_{c,j})(1-\mathbb{P}_{c,j}^{m-m'})\right)}, & m > m'. \end{cases} \tag{6}$$

Therefore, the probability of transmission in a mini-slot of the *jth* RAW slot is given by

$$\mathbb{P}_{t,j} = \sum_{i=0}^{m} \mathfrak{U}_{i,0} = \sum_{i=0}^{m} \mathbb{P}^i_{c,j} \mathfrak{U}'_{0,0} = \mathfrak{U}'_{0,0} \frac{1-\mathbb{P}^{m+1}_{c,j}}{1-\mathbb{P}_{c,j}}. \tag{7}$$

The probability that there is at least a transmission by anyone of $g-1$ devices in a mini-slot of the *jth* RAW slot is given by

[2]We consider $m = 5$, $R = 7$, $CW_{min} = 32$ and $CW_{max} = 1024$ according to [3].

[3]Although multiple packets can be sent in a TXOP, we assume only one packet for simplicity. Δ_{DATA} and Δ_{ACK} represent the time taken to transmit the data packet and acknowledgment corresponding to the MCS used.

$$\mathbb{P}_{c,j} = 1 - (1 - \mathbb{P}_{t,j})^{g-1}. \tag{8}$$

Equations (7) and (8) can be solved using numerical techniques. As a result, the probability of successful transmission in a mini-slot conditioned such that there is at least one transmission in a mini-slot of *jth* RAW slot is given by

$$\mathbb{P}_{s,j} = \frac{g\mathbb{P}_{t,j}\left(1 - \mathbb{P}_{t,j}\right)^{g-1}}{\mathbb{P}_{tr,j}}, \tag{9}$$

where $\mathbb{P}_{tr,j}$ is the probability of having at least one transmission in a mini-slot of *jth* RAW slot. Therefore

$$\mathbb{P}_{tr,j} = 1 - (1 - \mathbb{P}_{t,j})^{g}. \tag{10}$$

4.1 *Throughput analysis*

As shown in figure 5, Δ_h is defined as the holding time whose duration is at least equal to the duration of a TXOP, i.e., $\Delta_h = \xi - 1 + \Delta_g$, where Δ_g is the guard interval. During this period, start of a new transaction is prohibited because of NCR. Therefore, the effective period available to access the channel is $\Delta^{'}_{slot} = \Delta_{slot} - \Delta_h$. A transaction is the sum of TXOP, DIFS and the number of back-off slots before a TXOP. Let Δ_l be the duration of l transactions and represented as

$$\Delta_l = \sum_{i=1}^{l}(\xi^{'} + \mathfrak{B}_i), \tag{11}$$

where $\xi^{'} = \xi + \delta_d$ and $\mathfrak{B}_i$ is the number of back-off slots before *ith* transaction. The probability that a device takes b number of back-off slots before a transaction follows the geometric distribution with parameter $y' = 1 - (1 - \mathbb{P}_{t,j})^{g}$ and

$$\mathbb{P}\{\mathfrak{B} = b\} = y'(1 - y')^{(b-1)}. \tag{12}$$

Since the sum of l geometrically distributed variables $(\sum_{i=1}^{l} \mathfrak{B}_i)$ follows a negative binomial distribution, the probability that the duration of l transactions takes ψ mini-slots is given by

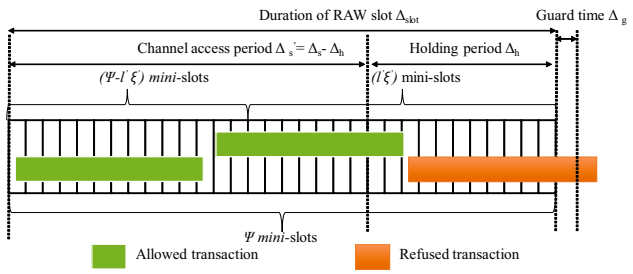

Figure 5. Illustration of no crossing slot case inside a RAW slot.

$$\begin{aligned}\mathbb{P}_{\Delta_l}(\psi) &= Prob\left\{\sum_{l'=1}^{l}\mathfrak{B}_{b,l'} = \psi - l'\xi'\right\} \\ &= \binom{\psi - l\xi' - 1}{\psi - l\xi' - l}(y'^{l})(1 - y')^{\psi - l\xi' - l}.\end{aligned} \tag{13}$$

The total number of transactions during $\Delta^{'}_{slot}$ is given by

$$\mathcal{T}_u = \left\lfloor \frac{\Delta^{'}_{slot}}{\xi' + \delta} \right\rfloor. \tag{14}$$

Let $\mathcal{M}$ be the random variable that indicates the number of transactions within $\Delta^{'}_{slot}$. Then the probability that there are l transactions within $\Delta^{'}_{slot}$ duration is given by

$$\mathbb{P}_j(\mathcal{M} \geq l) = \sum_{\psi=l}^{\Delta^{'}_{slot} - (l-1)\xi' - \delta_d - \rho} \binom{\psi - 1}{\psi - l}(y'^{l})(1 - y')^{\psi - l}. \tag{15}$$

From Eq. (15), the expected number of transactions within a *jth* RAW slot is given by

$$\mathbb{E}_j[\mathcal{M}] = \sum_{l=1}^{\mathcal{T}_u(\Delta_{slot} - \Delta_h)} l\ \mathbb{P}_j(\mathcal{M} \geq l). \tag{16}$$

Therefore, the network throughput is defined as the average number of successful transactions in a RAW slot:

$$S_j = \frac{K\ \mathbb{E}[Payload]}{\Delta_{RAW}}\mathbb{E}_j[\mathcal{M}]\mathbb{P}_{s,j}. \tag{17}$$

4.2 *Energy consumption analysis*

The energy consumption is defined as the average energy consumed during the successful transmission of a packet. In DCF mechanism, a device can be in either a back-off state, freezing state or a transmission state. Thus, each device consumes energy in four parts: E_b is the energy consumed during the back-off process; E_f is the energy consumed when a device freezes its back-off counter; E_s and E_c are the energies consumed due to a successful transmission and collision, respectively. The probability that a device senses the channel as busy during the $\Delta^{'}_{slot}$ is given by

$$\mathbb{P}_{b,j} = \frac{K\Delta^{'}_{slot}}{\Delta_{RAW}}(1 - (1 - \mathbb{P}_{t,j})^{g-1}). \tag{18}$$

The average energy consumed during the back-off process is given by

$$E_b = \mathbb{E}[B]\sigma P_{idle}, \tag{19}$$

where $\mathbb{E}[B]$ is the average number of back-off slots and is given by

$$\mathbb{E}[B] = \sum_{i=0}^{R} \mathbb{P}_{b,j}^{i}(1 - \mathbb{P}_{b,j}) \sum_{j=0}^{i} \frac{W_j - 1}{2}. \tag{20}$$

Among the g devices in a RAW slot, a node overhears a transmission when anyone of $g-1$ devices is successfully transmitting conditioned such that there is at least one transmission in the *jth* RAW slot. Therefore, the success probability is given by

$$\mathbb{P}_{s,j} = \frac{(g-1)\mathbb{P}_{t,j}\left(1 - \mathbb{P}_{t,j}\right)^{g-2}}{1 - (1 - \mathbb{P}_{t,j})^{g-1}}. \tag{21}$$

The average number of transmission overheard by a device during the back-off process is given by

$$N_0 = \frac{\mathbb{E}[B]\mathbb{P}_{b,j}}{1 - \mathbb{P}_{b,j}}. \tag{22}$$

Therefore, the energy consumed by a device due to overhearing the other nodes during the back-off process is given by

$$E_f = N_0[\mathbb{P}_{s,j}\xi' + (1 - \mathbb{P}_{s,j})(\xi - \Delta_{ACK})]P_{idle}. \tag{23}$$

Similarly, the average number of transmission attempts before a successful transmission is given by

$$N_t = \sum_{i=0}^{R} i\mathbb{P}_{b,j}^{i}(1 - \mathbb{P}_{b,j}). \tag{24}$$

Then the average energy consumed due to a successful transmission and collision is given by

$$\begin{aligned} E_s &= P_{Tx}\Delta_{DATA} + P_{Rx}\Delta_{ACK} + P_{idle}(\delta_s + \delta_d), \\ E_c &= N_t[P_{Tx}\Delta_{DATA} + P_{idle}(\delta_s + \delta_d)]. \end{aligned} \tag{25}$$

Therefore, the average energy consumed during the successful transmission of a packet in the *jth* RAW slot is given by

$$E_T = E_b + E_f + E_s + E_c. \tag{26}$$

Finally, the energy consumption per bit (η_j) is given by

$$\eta_j \approx \frac{E_T}{\mathbb{E}[Payload]}. \tag{27}$$

4.3 *Delay analysis*

The average delay (D_j) experienced by a device is equal to the time taken for successful transmission of a packet. This duration includes the average back-off delay, average delay due to a collision before the successful transmission and the duration of a packet transmission. Therefore

$$D_j = \mathbb{E}[B]\rho + N_t(\xi - \Delta_{ACK}) + \xi'. \tag{28}$$

5. ANN-based optimization framework

In this section, we develop an optimization framework using the ANN to find the optimal number of RAW slots that can maximize the performance of RAW mechanism. The optimal number of RAW slots K_{opt} is influenced by not only N but also the MCS used and Δ_{RAW}. As the correlation between them is non-linear and complex, solving Eq. (17) is time-consuming to find the optimal number of RAW slots. Hence, we propose ANN to model the non-linear functionality among the number of devices, MCS, duration of RAW period and the optimal number of RAW slots, and generalize it to the other inputs. MATLAB is used to solve the analytical model presented in the previous section by varying the N, MCS and Δ_{RAW}. The K_{opt} that can maximize the throughput and minimize delay and energy consumption is found for various values of N, MCS used and Δ_{RAW}. The inputs and outputs derived from the analytical model are used for training ANN. This procedure is summarized as follows.

Step 1: Find the K_{opt} for various N, MCS used and Δ_{RAW} using genetic algorithm in MATLAB.
Step 2: Train the ANN for different sets of (N, MCS used, Δ_{RAW}, K_{opt}).
Step 3: Once the ANN is trained, find the K_{opt} for any set of (N, MCS used, Δ_{RAW}).

We consider a feed-forward ANN that uses supervised learning to approximate the non-linear functions [33]. Supervised learning means the inputs and outputs are readily fed into the network to learn the correlation between them. Before discussing the proposed method, we briefly outline the gist of ANN's architecture. The basic architecture of the ANN has three layers, namely input, hidden and output layers, as shown in figure 6. Each layer has at least one artificial neuron as a fundamental processing element. All the neurons are connected directly within the layer and are connected to the neighbour layers with suitable weights and biases that determine the degree of correlation between them. The inputs are fed forward layer-by-layer up to the output. The ANN adaptively learns the non-linear relationship between the input and output variables and also updates the weights and biases by back-propagating the error between the actual output and the desired output iteratively. As shown in figure 6, the hidden layer has N neurons with M weights for M input elements $I = [i_1, i_2, ..., i_M]^T$ and P weights corresponding to P output elements $O = [o_1, o_2, ..., o_P]$. Therefore, the transfer function of the output layer is given by

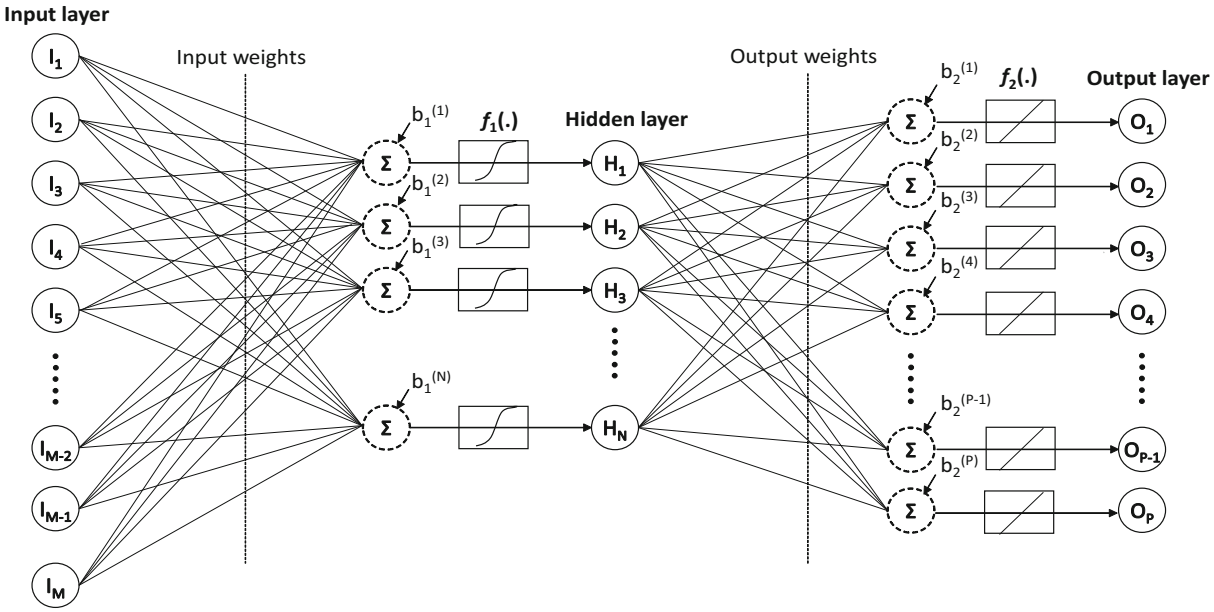

Figure 6. Architecture of Artificial Neural Network.

$$\begin{aligned}\mathbf{H} &= f(\mathbf{I_w I} + \mathbf{b1}),\\ \mathbf{O} &= f(\mathbf{O_w H} + \mathbf{b2}),\end{aligned} \tag{29}$$

where $f(.)$ is the activation function; $b1$ and $b2$ are the biases. W_{MN} and W_{NP} are the weights between the input–hidden layer and hidden–output layer, respectively. I_w and O_w are the weight matrices of input and output variables, respectively, and are given by

$$\mathbf{I}_w = \begin{bmatrix} w_{11} & w_{12} & \dots & w_{1M} \\ w_{21} & w_{22} & \dots & w_{2M} \\ & \dots\dots\dots & & \\ w_{N1} & w_{N2} & \dots & w_{NM} \end{bmatrix},$$
$$\mathbf{O}_w = \begin{bmatrix} w_{11} & w_{12} & \dots & w_{1P} \\ w_{21} & w_{22} & \dots & w_{2P} \\ & \dots\dots\dots & & \\ w_{N1} & w_{N2} & \dots & w_{NP} \end{bmatrix}. \tag{30}$$

The numbers of neurons in the input and output layer depend on the type of problem [9]. During the training phase of the neural network, the training data is fed to the input neurons and the corresponding output is calculated at the output layer according to Eq. (29). For every iteration, the ANN evaluates the difference between the actual output and desired output value at the output layer. This error is back propagated to update the respective weights and biases to minimize the error. The entire process repeats for every epoch till a predefined condition is satisfied. The training stops once the predefined condition is reached, and the ANN is now trained.

In this work, we implement ANN using MATLAB 9.4 neural network toolbox [34]. During the offline phase, the ANN is trained using the results obtained from the analytical model presented in the previous section. We use the Levenberg–Marquardt (LM) back propagation algorithm to improve the learning process of the neural network [35]. The Levenberg–Marquardt algorithm combines the Newton method and gradient descent method to update the weights and biases. We use the log sigmoid function $f_1(x) = (1+\exp(-x))^{-1}$ as an activation function at the hidden layer and a linear activation function $f_2(x) = x$ at the output layer. Knowing the fact that the number of neurons in the input and hidden layer should converge to the number of neurons in the output layer, we consider three neurons in the input layer corresponding to three inputs, i.e., N, MCS used and Δ_{RAW}, 20 neurons in the hidden layer and one neuron in the output layer corresponding to K_{opt}. The default parameters used to train the neural network are listed in table 3. The training process uses 70% of data for training, 15% for testing and the remaining for validation. The learning process stops when either the number of epochs is reached or performance goal is satisfied. During the online phase, the trained ANN is used to find the optimal number of RAW slots instead of solving computationally complex non-linear equations.

6. Results and discussion

In this section, we evaluate the performance of RAW mechanism in terms of throughput, delay and energy consumption using the proposed optimization framework

Table 3. Parameters used for analysis.

Payload	64 bytes
MAC header	14 bytes
T_{PLCP}	20 μs
ACK	14 bytes
ρ	52 μs
δ_s	160 μs
δ_d	264 μs
Δ_g	8 μs
RAW duration	500 ms
Beacon interval	Equal to RAW duration
Rate control algorithm	Constant
Wi-Fi mode	All MCS
P_{Tx}	255 mW
P_{Rx}	135 mW
P_{idle}	1.3 mW
Number of iterations	1000
Performance goal	1e–5

presented in the previous section. The results corresponding to the analytical model are obtained using MATLAB and validated through extensive ns-3 simulations. We consider various dense network scenarios in which large number of battery powered devices are uniformly deployed around the AP within the radius of 1000 m. The AP employs generic RAW mechanism with uniform grouping scheme. Since the number of groups is equal to the number of RAW slots in uniform grouping scheme, we consider $L_{opt} = K_{opt}$. The default parameters used to obtain the analytical and simulation results are listed in table 3.

Figure 7 shows the impact of varying group size on the throughput, delay and energy consumption in IEEE 802.11ah RAW mechanism. We consider four different networks scenarios with $N \in \{256, 512, 1024, 2048\}$. Let the duration of the RAW period be 500 ms and MCS0 be used for evaluation. As shown in figure 7a, the throughput gradually increases with an increase in the group size because of reduced contention among the group of devices. However, for larger values of K, the throughput decreases although the contention among the devices is reduced. The reason behind this phenomenon is twofold. First, the throughput performance is significantly affected when the transmission time of the data packet is shorter than the duration of the back-off counter. For example, let us consider the size of the network, and the number of groups be 256. Then the time taken to transmit a 64 bytes data packet using MCS3 is 787 μs, whereas the device wastes 832 μs ($\frac{CW_{min}}{2}\rho$) of channel time in the backup process. This unwanted phenomenon reduces the throughput of the network. Second, even though a single device is present in a group, it has to access the channel using GS-DCF, spending more number of mini-slots in the back-off process. It can be observed from figure 7a that the maximum throughput cannot be attained either at a lower K or at higher K. Hence,

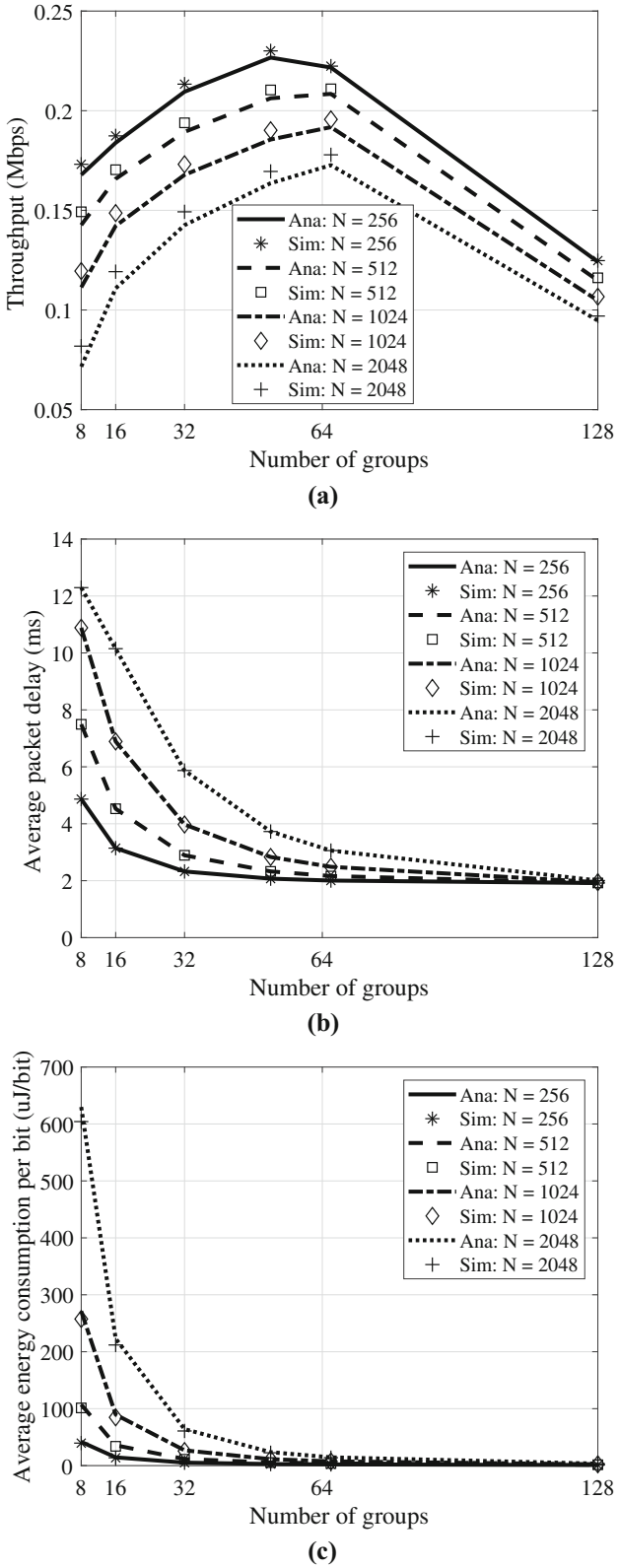

Figure 7. Performance of RAW mechanism vs number of groups: (a) throughput, (b) delay and (c) energy consumption.

the optimal number of RAW slots K_{opt} should be chosen to achieve the maximum performance of the RAW mechanism. Similarly, figure 7b and c shows that with an increase in the number of groups the delay and energy consumption decrease, due to the reduction in channel contention and wastage of channel resources.

To reduce the computational complexity involved in solving the non-linear equations, we adapt ANN to find the optimal number of RAW slots. The ANN model is trained using the network size, the duration of a RAW period, MCS and the optimal number of RAW slots. The ANN is trained with a learning rate of 0.01 till the number of epochs or the performance goal is reached. The trained module is similar to a black box with inputs and outputs that can be integrated into any wireless radio with minimum processing abilities [36]. To evaluate the performance of the proposed scheme, we compare the K_{opt} found using the proposed optimization framework to $K_{non-opt}$.

In figure 8, we access the performance of proposed scheme for different network sizes using K_{opt} and compare it to $K_{non-opt}$. We consider a network of size $N = 2048$ and $K_{non-opt} = \{16, 32\}$. The duration of the RAW period is $\Delta_{RAW} = 500$ ms. MCS0 is used for evaluation. The results show that with an increase in the value of N the throughput decreases, but shows maximum throughput performance at K_{opt} value. Similarly in figure 8b and c, the delay and energy consumption increase with N, but show optimum performance at K_{opt}. Choosing the optimal number of RAW slots not only mitigates the collisions among the devices but also decreases the wastage of channel resources, thereby increasing the efficiency of IEEE 802.11ah RAW mechanism. For larger value of K, the density of devices per group is high, which increases the collision, thus degrading the performance of the network in terms of throughput, delay and energy consumption. Hence, choosing the optimal number of RAW slots maximizes the throughput and minimizes the delay and energy consumption.

Figure 9 shows the performance of RAW mechanism with the variation of the data rates. We consider a network size of $N = 512$ devices divided into K_{opt} groups and the duration of the RAW period as $\Delta_{RAW} = 500$ ms. The results show that with the increase in data rate the throughput increases. Similarly in figure 9b and c, the delay and energy consumption decrease with an increase in the data rate. It can also be observed that maximum performance is achieved at K_{opt} rather than $K_{non-opt}$ due to the fact that the increase in data rate reduces the transmission time, which increases the number of transactions per RAW slot. Thus, the performance of RAW mechanism is enhanced. On the other hand, the optimum performance is achieved at K_{opt} due to the decrease in collisions and wastage of back-off slots. Table 4 shows the performance of RAW mechanism in terms of throughput, delay and energy consumption by varying the duration of the RAW period at regular intervals

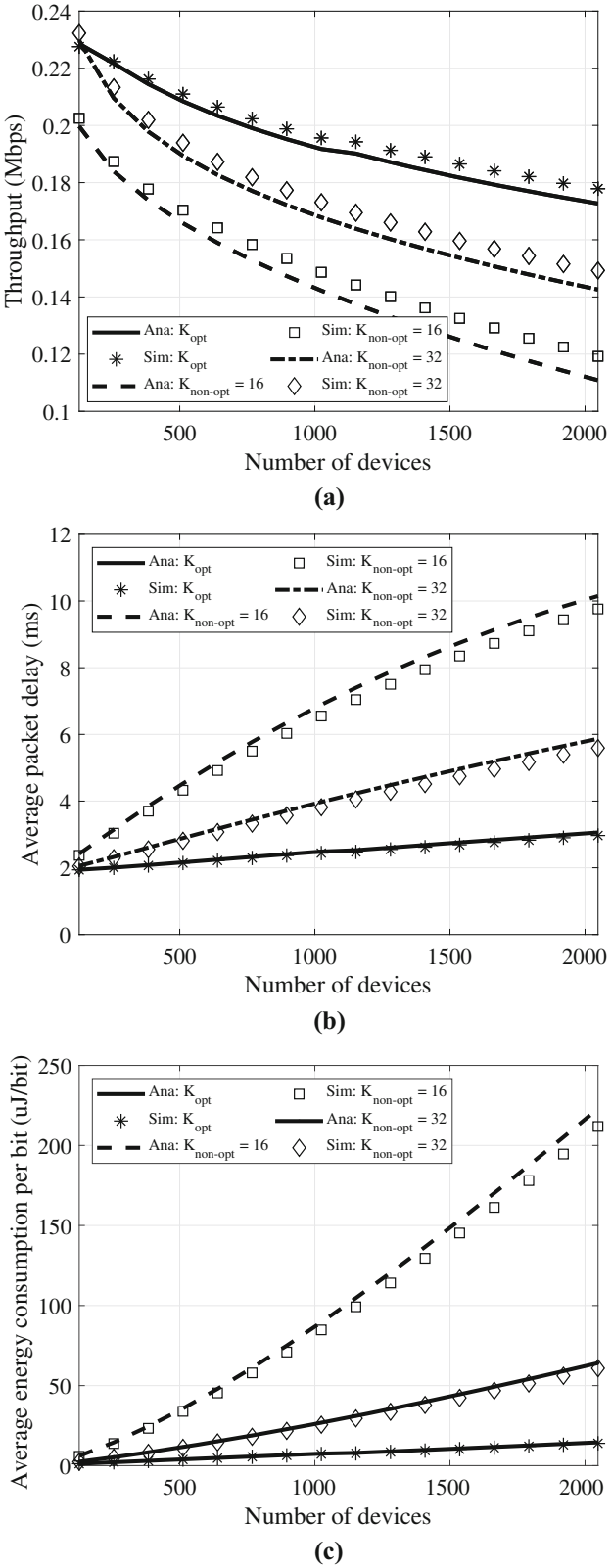

Figure 8. Performance of RAW mechanism vs number of devices: (a) throughput, (b) delay and (c) energy consumption.

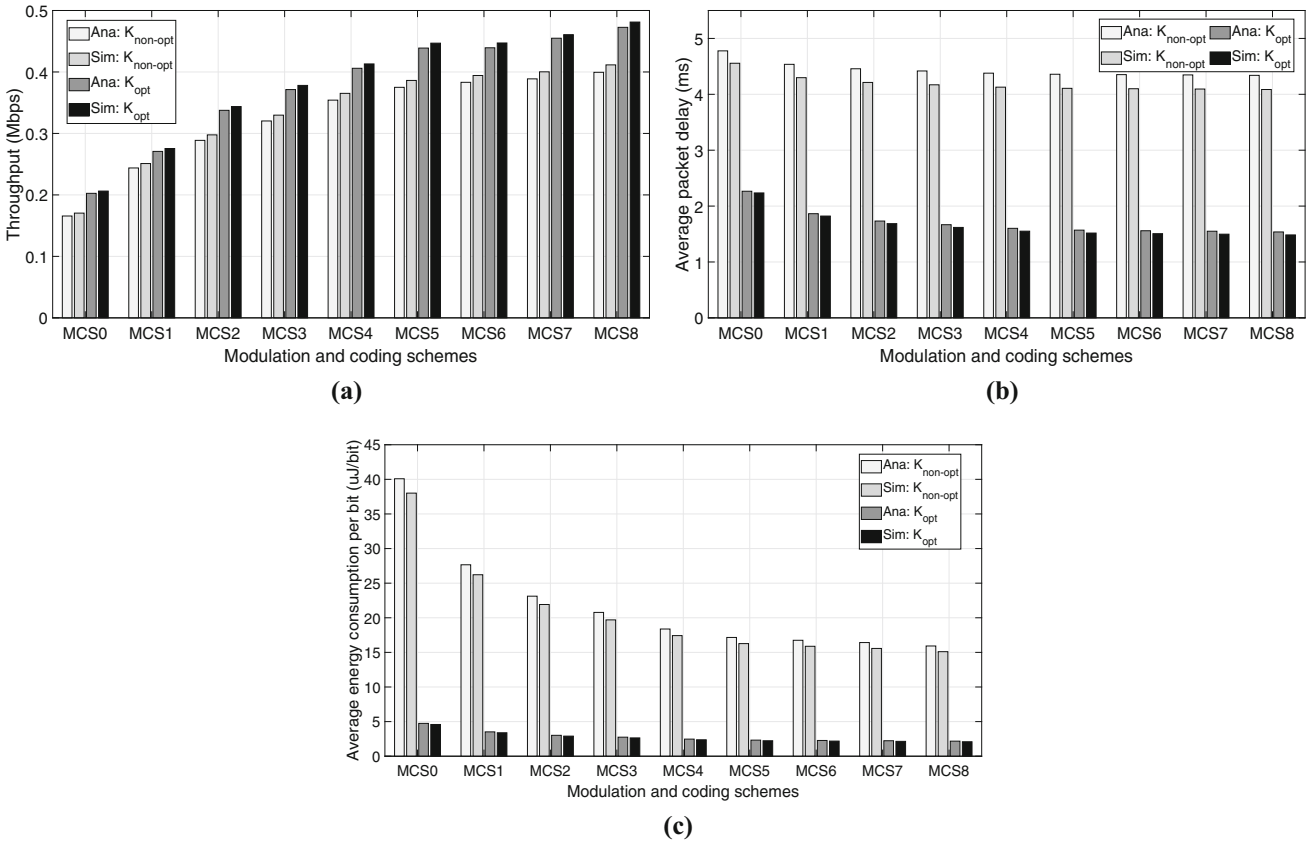

Figure 9. Performance of RAW mechanism vs Modulation and Coding Schemes: (a) throughput, (b) delay and (c) energy consumption.

Table 4. Performance of RAW mechanism in term of throughput, delay and energy consumption vs duration of RAW period.

			Duration of RAW (ms)									
			200		400		600		800		1000	
Parameter	Number of devices		$K_{non-opt}$	K_{opt}	$K_{non-opt}$	K_{opt}	$K_{non-opt}$	K_{opt}	$K_{non-opt}$	K_{opt}	$K_{non-opt}$	K_{opt}
Throughput (Mbps)	$N = 512$	Ana.	0.3551	0.4051	0.4146	0.4051	0.4144	0.4416	0.4144	0.4389	0.4143	0.4407
		Sim.	0.3636	0.4125	0.4244	0.4125	0.4243	0.4476	0.4243	0.4469	0.4242	0.4469
	$N = 1024$	Ana.	0.3147	0.3662	0.3688	0.3662	0.3679	0.4040	0.3681	0.3967	0.3676	0.4059
		Sim.	0.3246	0.3750	0.3799	0.3750	0.3792	0.4128	0.3793	0.4062	0.3790	0.4137
	$N = 2048$	Ana.	0.2674	0.3265	0.3171	0.3265	0.3154	0.3621	0.3161	0.3537	0.3150	0.3670
		Sim.	0.2799	0.3371	0.3306	0.3371	0.3291	0.3734	0.3296	0.3652	0.3287	0.3777
Delay (ms)	$N = 512$	Ana.	2.0879	1.2961	2.3892	1.4645	2.4814	1.5328	2.5313	1.5695	2.5625	1.5925
		Sim.	1.9999	1.2694	2.2735	1.4226	2.3571	1.4843	2.4023	1.5174	2.4306	1.5381
	$N = 1024$	Ana.	3.2070	1.6675	3.8688	2.0879	4.0711	2.2673	4.1804	2.3656	4.2487	2.4275
		Sim.	3.0445	1.6165	3.6544	1.9999	3.8412	2.1629	3.9420	2.2521	4.0052	2.3083
	$N = 2048$	Ana.	5.1246	2.2601	6.3474	3.1408	6.7092	3.5222	6.9019	3.7314	7.0214	3.8630
		Sim.	4.8440	2.1683	5.9927	2.9763	6.3347	3.3263	6.5174	3.5184	6.6309	3.6393
Energy consumption (uJ/bit)	$N = 512$	Ana.	4.3034	1.4162	5.6499	1.9598	6.0887	2.1943	6.3311	2.3239	6.4848	2.4060
		Sim.	4.1191	1.3752	5.3829	1.8895	5.7938	2.1102	6.0207	2.2320	6.1645	2.3090
	$N = 1024$	Ana.	9.7003	2.6530	13.7508	4.3034	15.1141	5.0892	15.8752	5.5399	16.3602	5.8309
		Sim.	9.2544	2.5617	13.0679	4.1191	14.3495	4.8572	15.0646	5.2798	15.5203	5.5524
	$N = 2048$	Ana.	22.3480	4.9709	33.5875	9.3405	37.4526	11.5682	39.6248	12.8769	41.0142	13.7324
		Sim.	21.2667	4.7750	31.8682	8.8953	35.5101	10.9884	37.5562	12.2165	38.8647	13.0188

Table 5. Comparison of K_{opt} found using different schemes.

	Optimal number of RAW slots K_{opt}				
Different schemes	$N = 16$	$N = 32$	$N = 64$	$N = 128$	$N = 256$
Simulated Annealing	8	8	21	52	66
Park's approach	6	12	23	50	62
ANN-based optimization	9	10	19	47	64

of 200 ms. We consider different networks of size $N \in \{512, 1024, 2048\}$ that uses MCS5. The result shows that the throughput, delay and energy consumption slightly increase with the increase in the duration of the RAW period because the increase in the duration of RAW period increases the number of transactions per slot. As the channel is effectively utilized at K_{opt}, the number of successful transactions increases, which in turn increases the throughput, delay and energy consumption. However, significant improvement in the performance of RAW mechanism is observed at K_{opt} rather than at $K_{non-opt}$.

Table 5 compares the optimal number of RAW slots found using ANN-based approach with the Simulated Annealing algorithm, and Park's approach based on [12]. We consider different networks of size $N \in \{16, 32, 64, 128, 256\}$ and use MCS0 for evaluation. The results in table 5 show the optimal number of RAW slots for all the three schemes. It is observed that K_{opt} found using the proposed scheme closely matches with the K_{opt} found using the other two schemes. Thus, the proposed optimization framework using ANN can provide the optimal number of RAW slots for various input conditions, which significantly improves the throughput performance of the IEEE 802.11ah RAW mechanism with lesser computational overhead.

7. Conclusion

In this paper, we have developed an optimization framework to find the optimal number of RAW slots using ANN. The ANN is trained with the network size, MCS, duration of RAW period and the optimal number of RAW slots obtained using the analytical model. We present a simple yet accurate analytical model to evaluate the performance of IEEE 802.11ah RAW mechanism in terms of throughput, delay and energy consumption. From the results, it is clear that the performance of RAW mechanism is significantly improved using the optimal number of RAW slots found using ANN. Extensive simulation studies have been conducted to validate the analytical findings.

List of symbols

N	Network size
n	Index of a device in the network
G	Number of groups
g	Index of a device in a group
Δ_{RAW}	Duration of RAW period
Δ_{slot}	Duration of RAW slot
ξ	Transmission Opportunity (TXOP)
ξ'	TXOP+DIFS
Δ_{DATA}	Time taken to transmit a data packet
Δ_{ACK}	Time take to transmit acknowledgment
δ_s	SIFS duration
δ_d	DIFS duration
ρ	Duration of mini-slot
m	Number of back-off stages
m'	Maximum re-transmission limit
$s(t)$	Stochastic process representing the back-off stage
$b(t)$	Stochastic process representing the back-off counter
l	Number of transactions
Δ_h	Duration of holding time
Δ_g	Guard interval
B_l	Number of back-off slots before *lth* transaction
Δ_l	Duration of l transactions
ψ	Number of mini-slot in a RAW slot
$\mathcal{T}_u$	Maximum number of transaction in a RAW slot

References

[1] Palattella M R, Accettura N, Vilajosana X, Watteyne T, Grieco L A, Boggia G and Dohler M 2013 Standardized protocol stack for the Internet of (important) things. *IEEE Commun. Surv. Tut*. 15(3): 1389–1406

[2] Kocan E, Domazetovic B and Pejanovic-Djurisic M 2017 Range extension in IEEE 802.11ah systems through relaying. *Wireless Pers. Commun*. 97(2): 1889–1910

[3] Man L A N, Standards Committee and IEEE Computer 2013 *IEEE Standard 802.11ac-2013: Part 11: Wireless LAN Medium Access Control (MAC) and Physical Layer (PHY) Specifications, Amendment 4 Enhancements for Very High Throughput for Operation in Bands below 6 GHz*.

[4] Ahmed N, Rahman H and Hussain M I 2018 An IEEE 802.11ah-based scalable network architecture for Internet of Things. *Ann. Telecommun*. 73(7): 499–509

[5] Wang C and Lin T 2008 Application of neural networks for achieving 802.11 QoS in heterogeneous channels. *Comput. Netw*. 52(3): 581–592

[6] Singh J P, Dutta P and Pal A 2012 Delay prediction in mobile ad hoc network using artificial neural network. In: *Procedia Technol*. 4: 201–206

[7] Wang C 2013 Dynamic ARF for throughput improvement in 802.11 WLAN via a machine-learning approach. *J. Netw. Comput. Appl*. 36(2): 667–676
[8] Lin P and Lin T 2009 Machine-learning-based adaptive approach for frame-size optimization in wireless LAN environments. *IEEE Trans. Veh. Technol*. 58(9): 5060–5073
[9] Afsharizadeh M and Mohammadi M 2016 Prediction-based reversible image watermarking using artificial neural networks. *Turk. J. Electr. Eng. Comput. Sci*. 24: 896–910
[10] Hornik K, Stinchcombe M and White H 1989 Multilayer feedforward networks are universal approximators. *Neural Netw*. 2(5): 359–366
[11] Hassoun M H 1995 *Fundamentals of artificial neural networks*, 1st ed. Cambridge, MA, USA: MIT Press
[12] Park C W, Hwang D and Lee T J 2014 Enhancement of IEEE 802.11ah MAC for M2M communications. *IEEE Commun. Lett*. 18(7): 1151–1154
[13] Khorov E, Lyakhov A, Krotov A and Guschin A 2015 A survey on IEEE 802.11ah: an enabling networking technology for smart cities. *Comput. Commun*. 58: 53–69
[14] Sun W, Choi M and Choi S 2013 IEEE 802.11ah: a long range 802.11 WLAN at sub 1 GHz. *J. ICT Standardiz.* 1: 1–26
[15] Adame T, Bel A, Bellalta B, Barcelo J and Oliver M 2014 IEEE 802.11ah: the WiFi approach for M2M communications. *IEEE Wireless Commun*. 21(6): 144–152
[16] Hazmi A, Rinne J and Valkama M 2012 Feasibility study of IEEE 802.11ah radio technology for IoT and M2M use cases. In: *Proceedings of the IEEE GLOBECOM Workshops*, pp. 1687–1692
[17] Aust S and Ito T 2012 Sub 1 GHz wireless LAN propagation path loss models for urban smart grid applications. In: *Proceedings of the International Conference on Computing, Networking and Communications (ICNC)*, pp. 116–120
[18] Casas R A, Papaparaskeva V, Mao X, Kumar R, Kaul P and Hijazi S 2015 An IEEE 802.11ah programmable modem. In: *Proceedings of the 2015 16th IEEE International Symposium on A World of Wireless, Mobile and Multimedia Networks (WoWMoM)*, pp. 1–6
[19] Yoon S G, Seo J O and Bahk S 2016 Regrouping algorithm to alleviate the hidden node problem in 802.11ah networks. *Comput. Netw*. 105: 22–32
[20] Damayanti W, Kim S and Yun J H 2016 Collision chain mitigation and hidden device-aware grouping in large-scale IEEE 802.11ah networks. *Comput. Netw*. 108: 296–306
[21] Dong M, Wu Z, Gao X and Zhao H 2016 An efficient spatial group restricted access window scheme for IEEE 802.11ah networks. In: *Proceedings of the 2016 Sixth International Conference on Information Science and Technology (ICIST)*, pp. 168–173
[22] Chang T C, Lin C H, Lin K C J and Chen W T 2015 Load-balanced sensor grouping for IEEE 802.11ah networks. In: *Proceedings of the 2015 IEEE Global Communications Conference (GLOBECOM)*, pp. 1–6
[23] Wang Y, Li Y, Chai K K, Chen Y and Schormans J 2015 Energy-aware adaptive restricted access window for IEEE 802.11ah based smart grid networks. In: *Proceedings of the 2015 IEEE International Conference on Smart Grid Communications (SmartGridComm)*, pp. 581–586
[24] Wang Y, Chai K K, Chen Y, Schormans J and Loo J 2017 Energy-aware Restricted Access Window control with retransmission scheme for IEEE 802.11ah (Wi-Fi HaLow) based networks. In: *Proceedings of the 2017 13th Annual Conference on Wireless On-demand Network Systems and Services (WONS)*, pp. 69–76
[25] Nawaz N, Hafeez M, Zaidi S A R, McLernon D C and Ghogho M 2017 Throughput enhancement of restricted access window for uniform grouping scheme in IEEE 802.11ah. In: *Proceedings of the 2017 IEEE International Conference on Communications (ICC)*, pp. 1–7
[26] Pandya B and Chiueh T D 2018 Interference aware coordinated multiuser access in multi-band WLAN for next generation low power applications. *Wireless Netw*. 25(4): 1965–1981
[27] Lei X and Rhee S H 2017 Performance improvement of Sub 1 GHz WLANs for future IoT environments. *Wireless Pers. Commun*. 93(4): 933–947
[28] Tian L, Famaey J and Latre S 2016 Evaluation of the IEEE 802.11ah Restricted Access Window mechanism for dense IoT networks. In: *Proceedings of the 2016 17th IEEE International Symposium on A World of Wireless, Mobile and Multimedia Networks (WoWMoM)*, pp. 1–9
[29] Wireless LAN Medium Access Control (MAC) and Physical Layer (PHY) specifications—amendment 4: enhancements for very high throughput for operation in bands below 6 GHz. *IEEE Std 802.11ac(TM)-2013*
[30] Adame T, Bel A, Bellalta B, Barcelo J, Gonzalez J and Oliver M 2013 Capacity analysis of IEEE 802.11Ah WLANs for M2M communications. In: *Proceedings of the 6th International Workshop on Multiple Access Communcations*, pp. 139–155
[31] Hsu C C and Liang S T 2017 An efficient retransmission mechanism for the RAW-based IEEE 802.11ah networks. In: *Proceedings of the 2017 International Conference on E-Society, E-Education and E-Technology*, pp. 8–11
[32] Chatzimisios P, Boucouvalas A C and Vitsas V 2003 IEEE 802.11 packet delay—a finite retry limit analysis. In: *Proceedings of the Global Telecommunications Conference, GLOBECOM '03*, IEEE, vol. 2, pp. 950–954
[33] Fausett L (Ed.) 1994 *Fundamentals of neural networks: architectures, algorithms, and applications*. Upper Saddle River, NJ, USA: Prentice-Hall, Inc.
[34] Demuth H and Beale M 1993 *Neural network toolbox for use with MATLAB*, http://www.mathworks.com/
[35] Lera G and Pinzolas M 2002 Neighborhood based Levenberg–Marquardt algorithm for neural network training. *IEEE Trans. Neural Netw*. 13(5): 1200–1203
[36] Zhai X, Ali A A S, Amira A and Bensaali F 2016 MLP neural network based gas classification system on Zynq SoC. *IEEE Access* 4: 8138–8146